CrossMark

# Novel Pt catalyst on ruthenium doped $TiO_2$ support for oxygen reduction reaction

N.R. Elezović [a],[*],[1], B.M. Babić [b], V.R. Radmilović [c], Lj.M. Vračar [c], N.V. Krstajić [c]

[a] Institute for Multidisciplinary Research, University of Belgrade, Kneza Viseslava 1, Belgrade, Serbia
[b] Vinča Institute of Nuclear Sciences, University of Belgrade, Serbia
[c] Faculty of Technology and Metallurgy, University of Belgrade, Belgrade, Serbia

## ARTICLE INFO

## ABSTRACT

Ruthenium doped titanium oxide support was synthesized. The support was characterized by BET (Brunauer, Emmett, Teller) and X-ray diffraction techniques (XRD). Determined specific surface area was $41\,m^2\,g^{-1}$. XRD revealed presence mainly $TiO_2$ anatase phase and some peaks belonging to rutile phase. No Ru compounds have been detected.

Platinum based catalyst on this support was prepared by borohydride reduction method. The catalyst was characterized by scanning transmission electron microscopy (STEM, HAADF) and electron energy loss spectroscopy (EELS). Homogenous Pt particle distribution over the support, with average Pt nanoparticle diameter of 3 nm was found. This novel catalyst was tested for oxygen reduction in acid solution. It exhibited remarkable higher catalytic activity in comparison with Pt/C, as well as with Pt nanocatalysts at titanium oxide based supports, reported in literature.

© 2013 Elsevier B.V. All rights reserved.

## 1. Introduction

Proton exchange membrane fuel cells (PEMFCs) are promising candidates for an environmental friendly and efficient energy conversion, with many prospective practical applications in portable, stationary and transport devices. Platinum based catalysts exhibit the best catalytic activity and stability for both reactions taking place in fuel cell: oxygen reduction and hydrogen oxidation [1–6]. High costs and scarce of Pt is a significant barrier to the mass application of this clean energy technology. The power loss at fuel cell cathode due to slow oxygen reduction kinetics is other limiting factor [7–9]. In contrast to fast hydrogen oxidation reaction on Pt, oxygen reduction reaction exhibits slow kinetics and much higher overpotential. In other words, the overall performance of fuel cell is much more influenced by oxygen reduction. Namely, thermodynamic reversible potential for oxygen reaction on Pt is 1.23 V vs. reversible hydrogen electrode, until the open circuit potential established vs. the same reference electrode is about 0.3 V lower. This large potential loss was attributed to the fact that the surface of Pt was covered with oxygen containing species from water (e.g. OH), or other adsorbed anions. Further improvement of fuel cell performance requires development of the catalyst more active for oxygen reduction. Other important point in a low temperature

PEMFC is catalyst support. Carbon based supports (commercially named Ketjen Black or Vulcan XC 72) are the most widely used owing to high conductivity and high surface area. However, oxidation of the carbon support during start/stop procedure, leads to degradation and decreases durability and life time of the fuel cell [1–3,10]. Nonstoichiometric mixture of several titanium oxide phases, mainly $Ti_4O_7$ and $Ti_5O_9$, known as Magneli phases or Ebonex, has been proposed as promising support material for Pt nanoparticles [11,12], as it posses high electrical conductivity and electrochemical stability in acid and alkaline solutions. The main disadvantage of Ebonex was low specific surface area. Slavcheva et al. referred the Ebonex specific surface area $2–3\,m^2\,g^{-1}$ [13]. Huang et al. reported high ORR activity Pt catalyst at niobium doped titanium oxide (rutile phase) support in acid solution [14].

Hass et al. reported binary oxide of ruthenium and titanium as a promising catalyst support for Pt, for fuel cells application, in acid solution [15]. Pt based catalyst on this support was synthesized by impregnation–reduction method and determined electrochemically active surface area was comparable to Pt on carbon support, assuming the same catalysts loading. However, the results for catalytic activity of oxygen reduction reaction were not presented [15].

Herein, Pt catalyst at ruthenium doped titanium oxide has been synthesized and characterized as a catalyst for oxygen reduction in acid solution. The synthesis way for the support, as well as for the Pt deposition, was different than that applied by Hass et al. [15]. The aim of this work was to investigate the effects of Ru doped titanium oxide on catalytic properties of Pt electrocatalyst for

* Corresponding author. Tel.: +381 11 3303 688; fax: +381 11 3055289.
  E-mail addresses: nelezovic@tmf.bg.ac.rs, elezovic@imsi.rs (N.R. Elezović).
[1] ISE member.

oxygen reduction in acid solutions. This catalyst exhibited remarkable enhancement of ORR activity, expressed in terms of specific and mass activity, compared to Pt/C, as well as Pt catalysts on titanium oxide based supports, referred in literature. Pt/C catalyst used for comparison of catalytic activities has been synthesized on commercial Vulcan XC 72 support.

## 2. Experimental

### 2.1. Preparation of Ru-doped TiO$_2$ support

Ru-doped TiO$_2$ powder was synthesized through a modified sol–gel route procedure proposed by Boujday et al. [16]. A procedure considers acid-catalyzed sol–gel method in a non-aqueous medium. Soles were prepared by adding a volume of 0.9 ml of 37% solution of hydrochloric acid (Zorka, Serbia) to a 40 ml of 97% solution of titanium (IV)isopropoxide, Ti[OCH(CH3)2]4, (Alfa Aesar, Germany), and an appropriate amount of a 1.7 g of RuCl$_3$ (Merck, Germany), previously dissolved in 10 ml of water, under vigorous steering (10% Ru in Ru/Ti atomic ratio to get the Ru$_{0.1}$Ti$_{0.9}$O$_2$ solid solution). Mixture was placed in glass tubes, sealed and placed 5 days at room temperature. In the presence of such amount of hydrochloric acid, the hydrolysis proceeded without forming a precipitate, leading to a transparent sol. Gellification of the sol was achieved by adding an appropriate amount of water.

The sample was dried by freeze–drying method using Modulyo Freeze Dryer System Edwards, England, consisting of freeze dryer unit at High Vacuum Pump E 2M 8 Edwards. Samples was prefrozen in deep-freeze refrigerator at −30 °C for 24 h. After that, sample was frozen drying in the acrylic chamber with shelves arrangements mounted directly on the top of the condenser of Freeze Dryer. The vacuum during twenty hours of freeze–drying was around 4 mbar.

Dried sample was heated to obtain anatase crystallized phase and to remove traces of organics in a conventional furnace, at 400 °C, for 2 h. After the treatment, the furnace was cooled at room temperature.

### 2.2. Preparation of Ru/TiO$_2$ supported Pt catalysts

Pt (20 wt.%) catalyst on Ru doped TiO$_2$ support was prepared by borohydride reduction method [17]. The main steps of this synthesis were following: appropriate amount of H$_2$PtCl$_6$ was dissolved in D.I. water. Ru/TiO$_2$ powder was dispersed in D.I. water and then mixed by adding platinum salt solution under constant stirring. The mixture of platinum salt and support was reduced by excess of sodium borohydride solution. Prepared precipitate was washed with water (18 MΩ) and then dried at 80 °C.

The Pt/C catalyst, with specific surface area of 92 m$^2$ g$^{-1}$, used as benchmark, was synthesized by modified ethylene glycol method on a commercial VulcanXC-72 support. The preparation procedure was fully described in Ref. [18].

### 2.3. Physical characterization of the support and catalyst

The support powder was also characterized by X-ray diffraction (XRD) technique on a Siemens D500 X-ray diffractometer using Cu Kα radiation with a Ni filter. The 2θ angular regions between 5 and 80° were explored at a scan rate of 0.02°/s with the angular resolution of 0.02° for all XRD tests.

TEM sample preparation included sonication of Pt/RuTiO$_2$ catalyst suspensions in ethanol for 5 min. After sonication, these suspensions were dropped on glassy carbon grids and dried in air. The samples were characterized for morphology, particle size distribution and chemical composition by high angle annular dark filed scanning transmission electron microscopy (HAADF, STEM)

and electron energy loss spectroscopy (EELS), using aberration corrected TEAM0.5 transmission electron microscope operated at 80 kV and 300 kV. HAADF was chosen because of its strong correlation between atomic number and image intensity making it very easy to distinguish between heavy elements such as Pt and light support such as Ru/TiO$_2$ particles. In order to account for the non-spherical shape, major and minor axes of all particles were measured, from which average particle diameters were extracted. A point energy dispersive spectroscopy (EDS) was performed on the CM200-FEG transmission electron microscope operated at 200 kV in the STEM mode using 1 nm beam size. High resolution phase contrast imaging (HREM) was performed by the Titan 80–300 kV noncorrected transmission electron microscope. Crystallographic information from individual Pt particles, such as the presence of facets, equilibrium shape, etc., was obtained by numerical Fourier filtering (FFT, Fast Fourier Transformation) of the digital image intensity spectra. All TEM characterization was done at the National Center for Electron Microscopy, Lawrence Berkeley National Laboratory.

### 2.4. Electrochemical characterization

Electrochemical measurements were performed in a conventional three-compartment glass cell, at the temperature of 25 °C, in 0.5 mol dm$^{-3}$ HClO$_4$ high-purity solution (Spectrograde, Merck), prepared in 18.2 MΩ pure water. The counter electrode was a platinum sheet of 5 cm$^2$ geometric area. A platinum plated Pt reversible hydrogen electrode (RHE) in the same solution and at the same temperature was used as the reference electrode.

The working electrode was gold rotating disk (diameter 5 mm, geometric surface area 0.196 cm$^2$). The ink was suspension of catalyst in ethanol and Nafion solution (5 wt.% Aldrich solution). It was first ultrasonically dispersed for 30 min. Aliquot of ink was transferred on the gold electrode and dried at 80 °C for 10 min to obtain thin film. The Pt loading was 8 μg (40 μg cm$^{-2}$ of Pt and 20 μg cm$^{-2}$ of Ru, per unit of the geometric surface area). Mayrhofer et al. [9] suggested that 42 μg$_{Pt}$ cm$_{disc}$$^{-2}$ is optimal loading for the fuel cell cathode. Namely, due to low Pt loading RDE could not be completely and homogenously covered. On the contrary, too high Pt loading implies that mass transport characteristics of the RDE are no longer satisfied.

The cyclic voltammetry experiments were performed in the potential range between hydrogen and oxygen evolution, in 0.5 mol dm$^{-3}$ HClO$_4$ solution, at sweep rate of 100 mV s$^{-1}$. During these experiments high purity nitrogen was continuously bubbling through the working electrode compartment. Linear sweep voltammetry, at rotation rate of ~1600 rpm and sweep rate of 20 mV s$^{-1}$ (positive going sweep was recorded), in the presence of pure oxygen gas in electrolyte, was applied for recording polarisation curves of oxygen reduction reaction.

Electrochemical measurements have been performed using potentiostat/galvanostat PAR Model 273.

## 3. Results and discussion

### 3.1. BET and XRD analysis

Ru-doped TiO$_2$ support has been characterized by BET (Brunauer, Emmett, Teller) and XRD techniques. The nitrogen adsorption isotherms were measured at RuTiO$_2$ support, at −196 °C, applying gravimetric Mc Bain method. Specific surface area, $S_{BET}$ = 41 m$^2$ g$^{-1}$, was determined. Nitrogen adsorption isotherm obtained on the support is presented in Fig. 1. It is obvious that this isotherm belongs to the IV type, according to YUPAC classification [19], associated to mesoporous type of materials. The
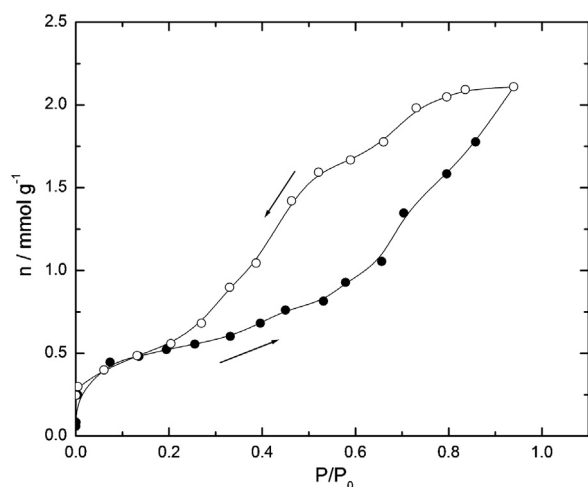
**Fig. 1.** Nitrogen adsorption isotherm for Ru/TiO$_2$ support: adsorption – solid symbol, desorption-Chem. Phys. open symbols.



**Fig. 3.** X-ray diffraction spectra of Ru/TiO$_2$ support.

hysteresis loop (the amount of adsorbed gas at a given relative pressure is larger on the desorption branch than on the adsorption branch) is caused by capillary condensation [20]. Pore size distribution of the support was estimated by the Barrett–Joyner–Halenda (BJH) method [21] and presented in Fig. 2. The maximum pore radius was about 2 nm (Fig. 2).

Typical XRD pattern for RuTiO$_2$ support is presented in Fig. 3. Observed peaks belong to anatase ($2\theta$ = 25.28°, 37.80°, 48.05° and 53.89°), or rutile ($2\theta$ = 27° and 36°) TiO$_2$ phase. All these peaks are in good accordance with the standard spectrum JCPDS No 88-1175 and 84-1286 [22]. No peaks corresponding to ruthenium compound were detected. The absence of any ruthenium belonging peaks indicates that average crystallite size is below the detection level of XRD technique and/or that the ruthenium is ultra fine dispersed on TiO$_2$ [23,24].

### 3.2. TEM analysis

Pt particles/clusters are uniformly distributed on Ru/TiO$_2$ particles, which are separated from each other by a network of nanopores. Ru/TiO$_2$ particle size was in the range between 5 and 30 nm. The typical overall distribution of metallic particles is shown in Fig. 4a. Fig. 4b shows a histogram of Pt particle size distribution (PSD).
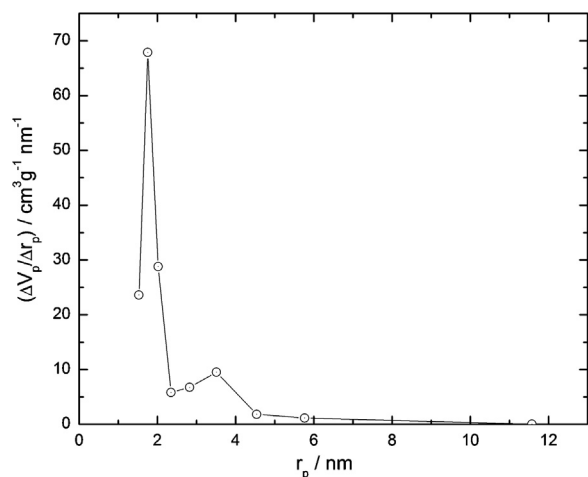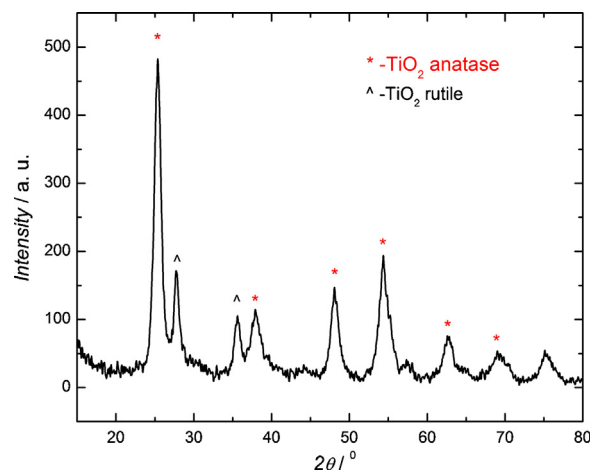


a



b



**Fig. 2.** Pore size distribution for Ru/TiO$_2$ support.
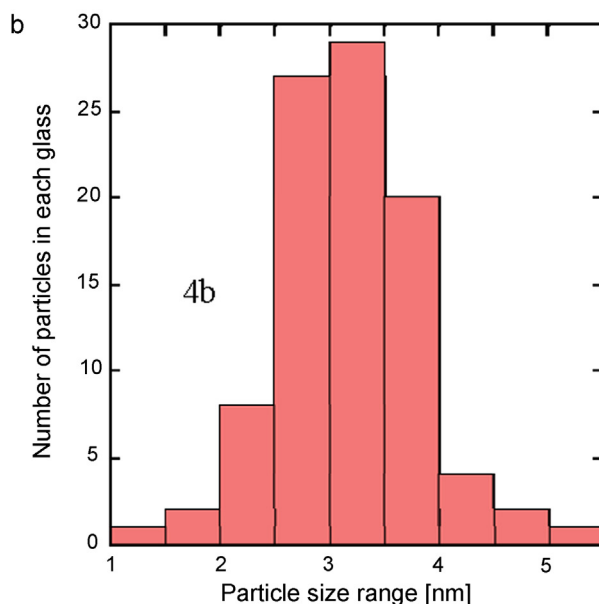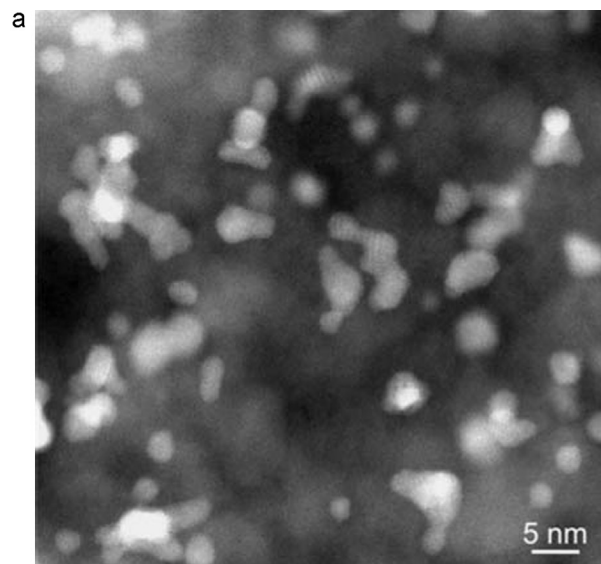
**Fig. 4.** (a) HAADF-STEM image of Pt particles/clusters on Ru/TiO$_2$ support; (b) histogram of Pt particle size distribution.
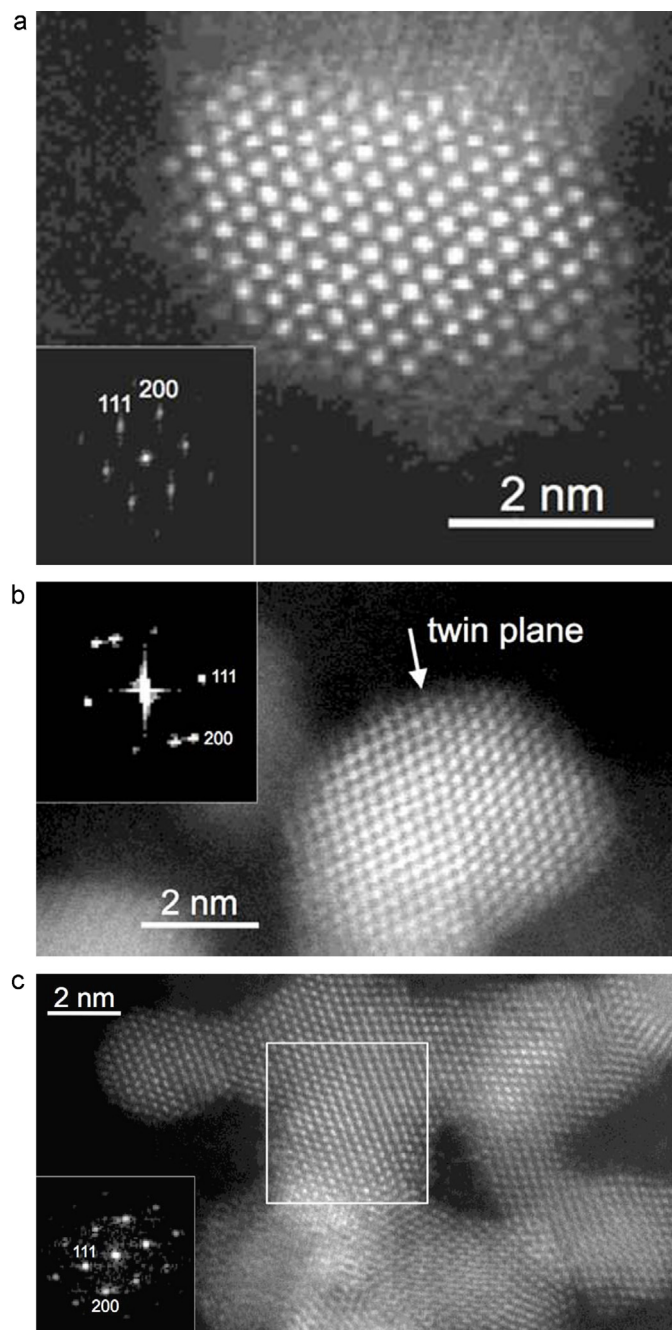
**Fig. 5.** HAADF images of: (a) Pt particle on Ru/TiO$_2$ substrate taken close to [1 1 0] zone axis. This particle exhibits clear faceting on 1 0 0 and 1 1 1 planes (see FFT inset in (a); (b) an example of twinned Pt particle, as shown by FFT inset in (b; (c) Pt particle cluster formed by the oriented attachment of individual Pt particles.



**Fig. 6.** (a) HREM image showing nucleation of Pt particle on 2 0 0 flat atomic plane of Ru/TiO$_2$ substrate; (b) FFT obtained from the white square in (a) and corresponding simulated diffraction pattern showing crystallographic orientation of Ru/TiO$_2$ close to [0 −2 1] zone axis.

The average Pt particle size obtained by the HAADF-STEM is around $3.1 \pm 0.32$ nm, similar to the one obtained from XRD. The typical shape of these Pt particles is cubooctahedron, as shown in Fig. 5a. However, examples of twinned particles were also observed, as shown in Fig. 5b. Pt is present either as individual particles or as particle clusters. It is interesting to note that cluster formation is taking place by the oriented attachment of individual Pt particles, as demonstrated in Fig. 5c. According to the recently published work [25], the cluster forming particles undergo continuous rotation until they find a perfect lattice match. Once the contact is established, further cluster growth proceeds by lateral atom-by-atom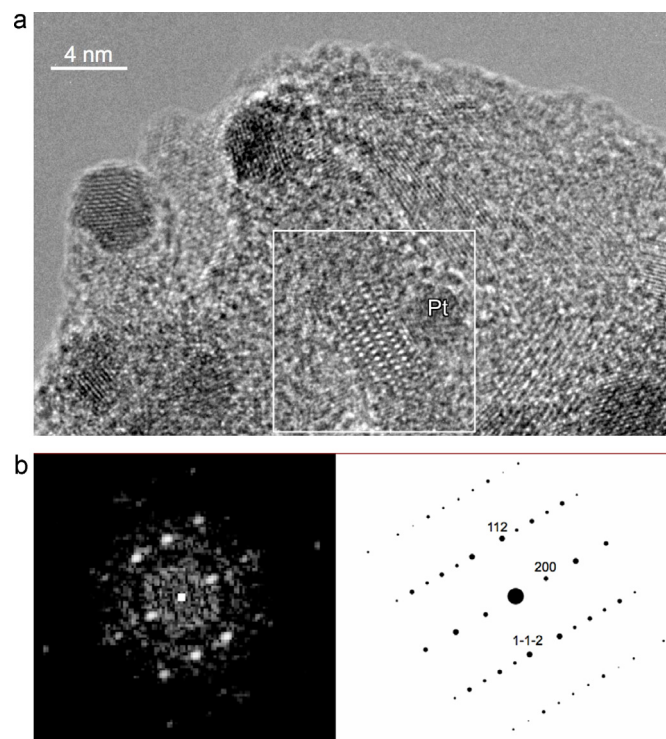 addition. A cluster which forms via this mechanism adopts a single crystal character. An example of such cluster made of Pt particles, imaged close to the [1 1 0] zone axis is shown in Fig. 5c.

Nucleation of Pt particles is always associated with Ru/TiO$_2$ particle substrate, as indicated in HREM image shown in Fig. 6a. FFT taken from the white square in Fig. 6a, shown in Fig. 6b, indicates that Pt particle can nucleate on 200 flat atomic plane of Ru/TiO$_2$ substrate. However, no crystallographic relationship between Pt particles and Ru/TiO$_2$ substrate has been observed.

### 3.3. Electrochemical characterization

Experimentally obtained cyclic voltammogram of Pt/RuTiO$_2$ in the potential range from 0 to 1.2 V vs RHE in 0.5 mol dm$^{-3}$ HClO$_4$ is presented in Fig. 7a. For comparison, the cyclic voltammogram of Pt/C catalyst, used as benchmark, is also presented, too (Fig. 7b). Typical platinum like shape, with well defined underpotential region of hydrogen and Pt—OH formation and reduction peaks has been observed (Fig. 7). Electrochemical active surface area (ECSA) was determined from cyclic voltammetry results, by integrating the anodic part of curve in the potential region of underpootential deposition of hydrogen, taking into account value of 210 μC cm$^{-2}$ for full monolayer coverage with adsorbed hydrogen species [26]. Correction for the double layer charge was applied, when calculation of the ECSA was performed. This calculation gave 30 m$^2$ g$^{-1}$ of Pt. Assuming spherical shape of the particles and knowing density of Pt (21.45 g cm$^{-3}$), the specific surface area of Pt for Pt/Ru-TiO$_2$ catalyst, based on TEM analysis (3 nm particle size) can be calculated as follows:

$$s_{Pt} = \frac{3}{r \times \rho} = \frac{3}{(3 \times 10^{-7}\,\text{cm}) \times (21.45\,\text{g cm}^{-3})} = 46.6\,\text{m}^2\text{g}^{-1} \quad (1)$$

It can be seen that obtained value is higher than electrochemically active surface area obtained from cyclic voltammetry. This could be explained by the presence of some agglomerated Pt
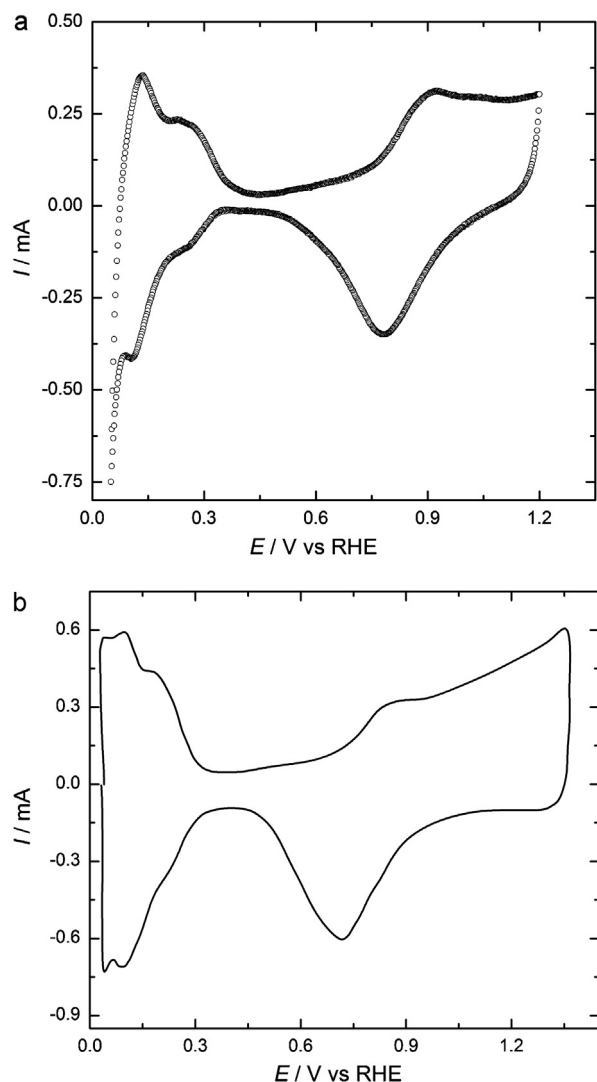
**Fig. 8.** Polarization curves for oxygen reduction at Pt/C and Pt/RuTiO$_2$ rotating disc electrodes, in oxygen saturated 0.5 mol dm$^{-3}$ HClO$_4$, sweep rate 20 mV s$^{-1}$, rotation rate 1652 rpm, and temperature 25 °C. Current densities are normalized to the geometric surface area.

**Fig. 7.** Cyclic voltammograms obtained with the Pt/RuTiO$_2$ electrode (a) and Pt/C electrode (b), in N$_2$ saturated 0.5 mol dm$^{-3}$ HClO$_4$; sweep rate of 100 mV s$^{-1}$ and temperature 25 °C.

particles, besides well dispersed particles at support, leading to lower utility efficiency of the catalyst. Agglomeration of Pt particles is probably caused by relatively low specific surface area of the Ru/TiO$_2$ support.

The oxygen reduction curves, obtained at rotating disc electrode, at 1652 rpm in 0.5 mol dm$^{-3}$ HClO$_4$ solution, for Pt/RuTiO$_2$ and Pt/C catalysts are presented in Fig. 8. It can be seen that at both catalysts almost the same diffusion limiting current density (expressed per geometric surface area) at the constant rotation rate was achieved (close to 4 mA cm$^{-2}$, about 10% discrepancy is within acceptable experimental error). This fact is indication of proper catalyst loading. It is obvious that Pt/RuTiO$_2$ catalyst exhibited remarkable higher activity in terms of onset potential and half wave potential. The onset potential and half wave potential are shifted to more positive potentials by ~45 mV.

In order to compare catalytic activity in terms of kinetic current density at the constant potential of practical importance (0.85 or 0.90 V vs RHE), the measured currents were corrected for mass transport influence, using Levich–Koutecky equation:

$$j^{-1} = j_k^{-1} + (B\omega^{1/2})^{-1} \qquad (2)$$

where: $j$ is measured current density, $j_k$ is kinetic current density and $B\omega^{1/2}$ is diffusion limiting current density. Mass transfer
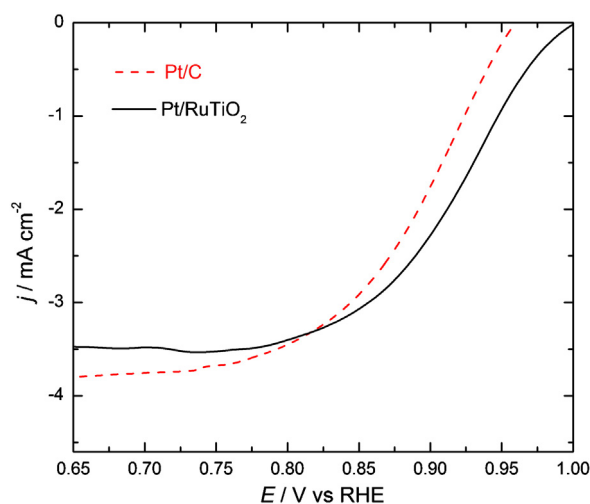
contribution corrected Tafel plots (dependence of the potential on log of kinetic current density) for Pt/C and Pt/RuTiO$_2$ are presented in Fig. 9. Two different Tafel slopes were observed, at low current densities close to 60 mV dec$^{-1}$, at high current densities close to 120 mV dec$^{-1}$, suggesting the same mechanism of the reaction with the transition in the Tafel slope related to the change in the nature of adsorbed oxygen containing species and their coverage variation with potential [27,28]. In addition to blocking of the Pt sites, according to Markovic at al. (8( the adsorbed OH has an energetic effect on the kinetics of oxygen reduction, too, through the change of Gibbs energy of adsorption of oxygen reduction intermediates by adsorbed OH.

Comparison of the catalytic activities for Pt/RuTiO$_2$, Pt/C and different Pt catalysts on titanium oxide based supports is presented in Table 1. Obtained values for specific and mass activity of Pt/C catalyst (Table 1), used for comparison, are in good accordance with widely accepted activity benchmarks for oxygen reduction reaction at carbon supported Pt catalysts in acid solutions [29]. It could be seen that Pt/RuTiO$_2$ catalyst exhibited remarkable enhancement in catalytic activity for oxygen reduction in terms of specific activity, as well as mass activity. Catalytic activity improvement could be
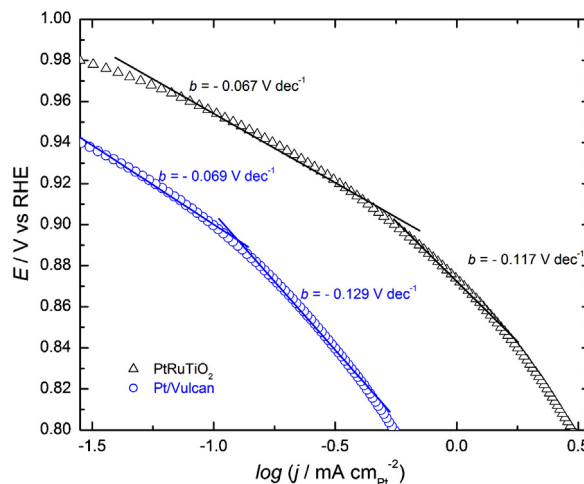


**Fig. 9.** Tafel plots normalized to the electrochemically active surface area for oxygen reduction at Pt/C and Pt/RuTiO$_2$ catalysts, in 0.5 mol dm$^{-3}$ HClO$_4$ solutions, at 25 °C.

**Table 1**
Specific and mass activities for different Pt catalysts on titanium oxide based supports and Pt/C catalyst at the constant potential.

| Catalyst | Electrochem. active surface area ($m^2 g^{-1}$ Pt) | Mass activity (mA/mg Pt) at $E/V$ vs RHE | | Specific activity ($\mu A/cm^2$ Pt) at $E/V$ vs RHE | |
|---|---|---|---|---|---|
| | | 0.85 | 0.90 | 0.85 | 0.90 |
| Pt/C[a] | 92 | 243 | 94 | 265 | 102 |
| Pt/RuTiO$_2$[a] | 30 | 460 | 167 | 1545 | 558 |
| Pt/Ebonex [30][a] | 36 | 219 | | 610 | |
| Pt/TiNbO$_x$ [32][b] | 94 | | 160 | | 170 |
| Pt/NbTiO$_2$ [33][a] | 42.5 | 172 | | 405 | |
| Pt/10NbTiO$_2$ [34][c] | | | | 178 | |

[a] Oxygen saturated 0.5 mol dm$^{-3}$ HClO$_4$, sweep rate of 20 mV s$^{-1}$.
[b] Oxygen saturated 0.1 mol dm$^{-3}$ HClO$_4$, sweep rate of 5 mV s$^{-1}$.
[c] Oxygen saturated 0.5 mol dm$^{-3}$ H$_2$SO$_4$, sweep rate of 5 mV s$^{-1}$.

explained by synergetic effect between the platinum particles and support and/or significant increase of the number of active Pt sites, probably through the change of electronic structure of the catalyst, connected to the metal–support interactions. Namely, the support could affect electronic structure of the catalysts, due to so called strong catalyst support interaction (SCSI) [30,31].

It should be emphasized that experimental conditions for oxygen reduction at all listed catalyst in Table 1 are not completely the same. Namely, the experimental conditions for oxygen reduction investigations at Pt/C, Pt/RuTiO$_2$, Pt/Ebonex and Pt/NbTiO$_2$ catalysts were exactly the same.

The parameter that is the most influenced by different concentration of the acid electrolytes is diffusion limiting current density of oxygen reduction. For instance, in 0.1 mol dm$^{-3}$ HClO$_4$ solution, at 1600 rpm rotation rate, theoretical value of diffusion limiting current density should be close to 6 mA cm$^{-2}$, while in 0.5 mol dm$^{-3}$ HClO$_4$ at the same rotation rate is close to 4 mA cm$^{-2}$, which is almost the same to diffusion limiting current density for oxygen reduction in 0.5 mol dm$^{-3}$ H$_2$SO$_4$, expressed per geometric surface area. However, kinetic current densities used for comparison in all cases are determined after diffusion contribution correction, according to Levich–Koutecky equation and expressed per real electrochemically active surface area. Different sweep rates are also usually applied for recording oxygen reduction polarization curves at Pt based catalysts in the literature.

The enhanced catalytic activity of the Pt/Ru-TiO$_2$ catalyst could be also explained as follows: change of oxygen adsorption conditions, through the change of electronic structure of the catalyst, related to the electronic interactions between platinum and the supportive material, could be caused by increase of 5d vacancy of Pt and decrease of Pt—Pt bond distances. According to density functional calculations of adsorption energies and activation barriers the reactivity of metal atom is determined by the location of the centre of the local d-bond relative to the Fermi level [33,35,36]. Generally, the change in the surface d-state induces changes in the interaction between the adsorbate valence states and the metal surface.

The hypo-d-electron transition metal oxides, such as TiO$_2$, exhibit strong metal support interaction (SMSI) [37], which can improve the activity of the Pt catalyst towards the ORR. The modification of the electronic structure of Pt nanoparticles by interaction with the oxide interface results in a change in the adsorption characteristics of Pt on Ru–TiO$_2$ support. According to Lin [38] in a Pt/TiO$_2$ electrode, the possibility of oxygen spillover and back spillover is identified. The electrochemical adsorption takes place on Pt active sites and oxygen containing species are quickly transferred directly from the Pt surface into the TiO$_2$ lattice (oxygen spillover).

The main role of ruthenium, added to titanium oxide support was to improve its conductivity. It is well known that TiO$_2$ is characterized by excellent chemical and corrosion stability in both acid and alkaline environment, however it belongs to semi conductive materials and conductivity should be improved by proper doping. On the other hand, Ru based catalysts have been reported as the catalysts for oxygen reduction reaction, too. However, Ru based catalysts exhibited much lower catalytic activities than Pt. The oxygen reduction at Ru-based catalysts does not take place in the same potential range like at Pt based catalysts. Namely, it is common to compare catalytic activities for oxygen reduction reaction between Pt based catalysts at 0.85 or 0.90 V vs RHE, where the same reaction at Ru based catalysts does not take place at all. It was reported that open circuit potential for oxygen reduction at Ru based catalysts is from 0.80 V to 0.85 V vs RHE, which makes it incomparable to Pt. Therefore, there is no Ru contribution to the Pt catalyst activity for oxygen reduction reaction in the potential range from 0.85 V to 0.90 V vs RHE [39–42].

## 4. Conclusion

In summary, in this manuscript novel platinum based catalyst on Ru doped TiO$_2$ support was successfully synthesized and characterized. XRD analysis revealed mainly presence of anatase TiO$_2$ phase and some peaks belonging to rutile TiO$_2$. BET analysis confirmed mesoporous nature of material, with specific surface area of 41 m$^2$ g$^{-1}$. Pt catalyst on this support has been prepared by borohydride reduction method. Homogenous particle distribution and average particle size about 3 nm were determined by TEM technique. This new catalyst exhibited remarkable enhanced catalytic activity for oxygen reduction reaction in acid solution, compared to Pt/C, as well as to literature values for Pt catalysts on titanium oxide based supports.

## References

[1] M.T. Paffet, K.A. Daube, S. Gottesfeld, T.C. Campbell, Journal of Electroanalytical Chemistry 220 (1987) 269–285.

[2] M.T. Peffet, J.G. Beery, S. Gottesfeld, Journal of the Electrochemical Society 135 (1988) 1431–1436.

[3] T. Toda, H. Igarashi, H. Uchida, M. Watanabe, Journal of the Electrochemical Society 146 (1999) 3750–3756.

[4] S. Zhang, Y. Shao, G. Yin, Y. Lin, Applied Catalysis B: Environmental 102 (2011) 372–377.

[5] T. Kottakkat, A.K. Sahu, S.D. Bhat, P. Sethuraman, S. Parthasarathi, Applied Catalysis B: Environmental 110 (2011) 178–185.

[6] D. Sebastian, A.G. Ruiz, I. Suelves, R. Moliner, M.J. Lazaro, V. Baglio, A. Stassi, A.S. Arico, Applied Catalysis B: Environmental 115–116 (2012) 269–275.

[7] A. Damjanovic, D.B. Sepa, Electrochimica Acta 35 (1990) 1157–1162.

[8] N.M. Markovic, H.A. Gasteiger, P.N. Ross, Journal of Physical Chemistry 100 (1996) 6715–6721.

[9] K.J.J. Mayrhofer, D. Strmcnik, B.B. Blizanac, V. Stamenkovic, M. Arenz, N.M. Markovic, Electrochimica Acta 53 (2008) 3181–3188.

[10] C.A. Reiser, L. Bregoli, T.W. Patterson, S.Yi. Jung, J.D. Yang, M.L. Perry, T.D. Jarvi, Electrochemical and Solid-State Letters 8 (2005) A273–A276.

[11] E.E. Farndon, D. Pletcher, Electrochimica Acta 42 (1997) 1281–1285.

[12] G.R. Dieckmann, S.H. Langer, Electrochimica Acta 44 (1998) 437–444.

[13] E. Slavcheva, V. Nikolova, T. Petkova, I. Dragieva, T. Vitanov, E. Budevski, Electrochim.Acta 50 (2005) 5444–5448.

[14] S.Y. Huang, P. Ganesan, B.N. Popov, Applied Catalysis B: Environmental 96 (2010) 224–231.

[15] O.E. Hass, S.T. Briskeby, O.E. kongstein, M. Tsypkin, R. Tunold, B.T. Barresen, Journal of New Materials for Electrochemical Systems 11 (2008) 9–14.

[16] S. Boujday, F. Wunsch, P. Portes, J.F. Bocquet, C. Colbeau-Justin, Solar Energy Materials & Solar Cells 83 (2004) 421–433.

[17] K.W. Park, K.S. Seul, Electrochemistry Communications 9 (2007) 2256–2260.

[18] B.M. Babic, Lj.M. Vracar, V. Radmilovic, N.V. Krstajic, Electrochimica Acta 51 (2006) 3820–3826.

[19] K.S.W. Sing, D.H. Everett, R.A.W. Haul, L. Moscou, R.A. Pierotti, J. Rouquerol, T. Siemieniewska, Pure and Applied Chemistry 57 (1985) 603–619.

[20] M. Sheykhan, A. Heydari, L. Mamani, A. Badiei, Spectrochimica Acta. Part A, Molecular and Biomolecular Spectroscopy 83 (2011) 379–383.

[21] E.P. Barrett, L.G. Joyner, P.P. Halenda, Journal of the American Chemical Society 73 (1951) 373–380.

[22] K. Thamaphat, P. Limsuwan, B. Ngotawornchai, J. Kasetsart, Nature Science 42 (2008) 357–361.

[23] S.S. Kim, B. Kwon, J. Kim, Catalysis Communications 8 (2007) 2204–2207.

[24] K. Wetchakun, S. Phanichphant, Journal of Microscopy Society of Thailand 22 (2008) 11–14.

[25] D. Li, M.N. Nielsen, J.R.I. Lee, C. Frandsen, J.F. Banfield, J.J. De Yoreo, Science 336 (2012) 1014–1018.

[26] J.T. Hwang, J.S. Chung, Electrochimica Acta 38 (1993) 2715.

[27] A. Damjanovic, A. Dey, J.O.M. Bockris, Electrochimica Acta 11 (1966) 791–814.

[28] D.B. Sepa, M.V. Vojnovic, Lj. Vracar, A. Damjanovic, Electrochimica Acta 31 (1986) 91–96.

[29] H.A. Gasteiger, S.S. Kocha, B. Sompalli, F.T. Wagner, Applied Catalysis B: Environmental 56 (2005) 9–35.

[30] Lj.M. Vračar, N.V. Krstajić, M.M. Jakšići, V.R. Radmilović, Journal of Electroanalytical Chemistry 587 (2006) 99–107.

[31] M. Jaksic, Electrochimica Acta 45 (2000) 4085–4099.

[32] T.B. Do, M. Cai, M.S. Ruthkosky, T.E. Moylan, Electrochimica Acta 55 (2010) 8013–8017.

[33] N.R. Elezović, B.M. Babić, Lj. Gajić-Krstajić, V. Radmilović, N.V. Krstajić, Lj. Vračar, Journal of Power Sources 195 (2010) 3961–3968.

[34] H. Chhina, S. Campbell, O. Kesler, Journal of the Electrochemical Society 156 (2009) B1232–B1237.

[35] B. Hammer, J.K. Norskov, Advances in Catalysis 45 (2000) 71–129.

[36] A. Ruban, B. Hammer, P. Stoltze, H.L. Skriver, J.K. Norskov, Journal of Molecular Catalysis A 115 (1997) 421–429.

[37] S. Meyer, S. Saborowski, B. Schafer, ChemPhysChem 7 (2006) 572–574.

[38] H. Lin, Journal of Molecular Catalysis A: Chemical 144 (1999) 189–197.

[39] R.G. Gonzalez-Huerta, J.A. Chavez-Carvayar, O. Solorza-Feria, Journal of Power Sources 153 (2006) 11–17.

[40] M. Bron, P. Bogdanoff, S. Fiechter, M. Hilgendorff, J. Radnik, I. Dorbandt, H. Schulenburg, H. Tributsch, Journal of the Electroanalytical Chemistry 517 (2001) 85–94.

[41] M. Hilgendorff, K. Diesner, H. Schulenurg, P. Bigdanoff, M. Bron, S. Fiecher, Journal of New Materials for Electrochemical Systems 5 (2002) 71–81.

[42] A. Altamirano-Gutierrez, O. Jimenez-Sandoval, J. Uribe-Godinez, R.H. Castellanos, E. Borja-Arco, J.M. Olivares-Ramirez, International Journal of Hydrogen Energy 34 (2009) 7983–7994.